Journal of the Korean Physical Society, Vol. 72, No. 11, June 2018, pp. 1379∼1386

Performance Evaluation and Quantitative Accuracy of Multipinhole NanoSPECT/CT Scanner for Theranostic Lu-177 Imaging

Arun Gupta, Kyeong Yun Kim, Donghwi Hwang, Min Sun Lee, Dong Soo Lee and Jae Sung Lee*
Department of Nuclear Medicine, College of Medicine, Seoul National University, Seoul 03080, Korea

(Received 26 March 2018, in final form 9 April 2018)

SPECT plays important role in peptide receptor targeted radionuclide therapy using theranostic radionuclides such as Lu-177 for the treatment of various cancers. However, SPECT studies must be quantitatively accurate because the reliable assessment of tumor uptake and tumor-to-normal tissue ratios can only be performed using quantitatively accurate images. Hence, it is important to evaluate performance parameters and quantitative accuracy of preclinical SPECT systems for therapeutic radioisotopes before conducting pre- and post-therapy SPECT imaging or dosimetry studies. In this study, we evaluated system performance and quantitative accuracy of NanoSPECT/CT scanner for Lu-177 imaging using point source and uniform phantom studies. We measured recovery coefficient, uniformity, spatial resolution, system sensitivity and calibration factor for mouse whole body standard aperture. We also performed the experiments using Tc-99m to compare the results with that of Lu-177. We found that the recovery coefficient of more than 70% for Lu-177 at the optimum noise level when nine iterations were used. The spatial resolutions of Lu-177 with and without adding uniform background was comparable to that of Tc-99m in axial, radial and tangential directions. System sensitivity measured for Lu-177 was almost three times less than that of Tc-99m.

PACS numbers: 87.57.uh, 87.57.cm, 87.57.cf, 87.57.nf, 87.57.uq
Keywords: NanoSPECT/CT, Lu-177, Recovery Coefficient, Spatial Resolution, Sensitivity
DOI: 10.3938/jkps.72.1379

I. INTRODUCTION

Small animal single photon emission computed tomography/computed tomography (SPECT/CT) is widely used nowadays in preclinical research due to the possibility of translation of results from preclinical laboratories to the human clinical setting [1,2]. The SPECT image qualities are fundamentally dependent on collimator type as well as the reconstruction technique [3]. There has been significant progress in the development and application of small-animal SPECT using pinhole collimator however, the further research continues to address challenges in camera sensitivity, spatial resolution, image reconstruction and quantification [1]. The essential requirements of small animal-dedicated SPECT systems are high and uniform spatial resolution along the entire filed of views (FOVs) to assess small lesions and higher sensitivity to acquire images with better signal-to-noise ratio (SNR) [4]. However, there is a trade-off between high spatial resolution and low sensitivity when using small-animal SPECT with pinhole collimator [1,5, 6]. Number of approaches have been proposed to solve this issue and consequently, researchers have designed SPECT camera with multipinhole collimators that increases the system sensitivity while maintaining good spatial resolution [2,5,7–9].

Most commercially available small-animal SPECT scanners today (Bioscan NanoSPECT, GE Triumph X-SPECT, MILabs U-SPECT-II, and Siemens Inveon SPECT) use multipinhole collimation [10]. The NanoSPECT/CT (Bioscan Inc., Washington D.C., USA) is a multipinhole four headed small-animal SPECT imaging system which has shown good sensitivity while achieving high, even submillimetre, resolution [8,11–13]. Phantom and preclinical imaging studies were performed by different researchers to evaluate the NanoSPECT camera performance using various diagnostic radioisotopes [8,12–15]. Schramm *et al.* [8] measured the spatial resolution and sensitivity of NanoSPECT camera using phantom and small-animal imaging for Tc-99m, I-123 and In-111 tracers. Ciara *et al.* [14] performed phantom imaging using In-111 and Tc-99m sources and concluded that the NanoSPECT camera is quantitatively accurate and allows replacement of dissection studies for the assessment of radiotracer biodistribution in mouse models.

SPECT plays a fundamental role in targeted radionuclide therapy (TRT) using theranostic radionuclides like I-131, Re-188 and Lu-177 [16,17]. Particularly, peptide receptor TRT with Lu-177 has gained an established role

*E-mail: jaes@snu.ac.kr; Fax: +82-2-2072-2938

in the treatment of various cancers including neuroendocrine tumors [18–23]. Lu-177 has several advantages: (a) emits low-energy beta emissions that shows efficient cross fire effects; (b) favorable half-life; (c) gamma emissions of adequate energy to perform imaging studies to evaluate radiotracer biodistribution [24]. The published studies show promising results in terms of treatment outcome from patients treated with Lu-177 using fixed activities however, it is expected that personalized dose assessment could further improve the clinical outcomes in terms of the tumor control and reduction of the normal tissue effects [22–25]. During personalized dosimetry, both pre- and post-therapy SPECT studies must be quantitatively accurate because reliable assessment of tumor uptake and tumor-to-normal tissue ratios can only be performed using quantitatively accurate images [26]. Hence, it is very important to evaluate performance parameters of preclinical SPECT systems for therapeutic radioisotopes before conducting pre- and post-therapy SPECT imaging or dosimetry studies.

Several studies have been performed by different authors to evaluate the performance parameters of clinical SPECT/CT system for Lu-177 radionuclide however, there is no such study available for preclinical SPECT system using Lu-177 yet. In this study, we conducted series of point source imaging and uniform phantom studies using Lu-177 and Tc-99m sources to evaluate the quantitative accuracy and performance parameters of multipinhole mouse aperture of NanoSPECT/CT system. We measured recovery coefficient, uniformity, reconstructed spatial resolution and system sensitivity using both Lu-177 and Tc-99m. In addition, we measured calibration factor of mouse aperture of NanoSPECT/CT system for Lu-177. We also compared the spatial resolution measured with and without adding uniform background to the point source data before image reconstruction.

II. EXPERIMENTS

1. NanoSPECT/CT system

The NanoSPECT/CT (Bioscan Inc., Washington D.C., USA) is a multipinhole four-headed small-animal SPECT imaging system. NanoSPECT/CT comes with series of dedicated multipinhole aperture suitable for imaging both mouse and rat using different diagnostic and therapeutic radioisotopes [12]. In this study, we used mouse whole body standard aperture (NSP-108-M14-WB) for SPECT imaging of point source and uniform phantom using both Lu-177 and Tc-99m. The axial and transaxial field of views (FOVs) for this mouse aperture are 14 mm and 30 mm respectively. The aperture has nine pinhole of 1.4 mm diameter. There are total 36 pinholes of four apertures mounted at four heads of the scanner. The NanoSPECT/CT system has detector size

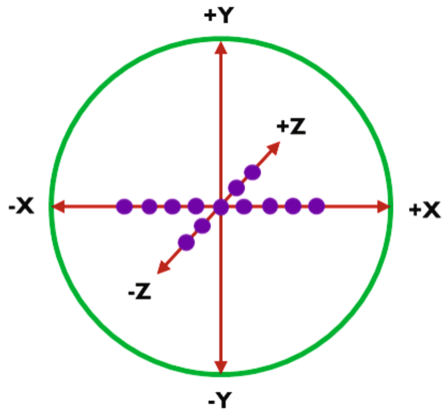

Fig. 1. (Color online) Point source projections data were acquired at the center of axial and transaxial FOV and repeated at every 2 mm from the center. Axial FOV: 14 mm; Transaxial FOV: 30 mm.

of 350 mm × 345 mm made up of NaI (Tl). It consists of 33 circular photo-multiplier tubes (PMTs) each of 2 inches in size. It also incorporates a cone beam CT for volumetric imaging through helical scanning.

2. Point source acquisition

In this study, we used capillary tube having internal diameter of 1.1 mm to prepare point sources of Lu-177 and Tc-99m. The activities in the Lu-177 and Tc-99m point sources were 1.78 MBq and 1.59 MBq respectively. Since the activities in the point sources were very low, the background was corrected in dose calibrator before measuring activities. Three different energy windows (20% width) were adopted for Lu-177: 208.4 ± 20.84 keV, 112.9 ± 11.29 keV, and 56.30 ± 5.63 keV. For Tc-99m, 20% window was centered at 140 keV photopeak. First, the SPECT data image was acquired with Lu-177 point source placed at the center of the axial and transaxial FOVs and repeated at every 2 mm from the center. We acquired point source projection data at total 5 positions (-4 mm, -2 mm, center, $+2$ mm, $+4$ mm) in axial and 9 positions (-8 mm, -6 mm, -4 mm, -2 mm, center, $+2$ mm, $+4$ mm, $+6$ mm, $+8$ mm) in transaxial FOVs as shown in Fig. 1. The whole procedures were repeated with Tc-99m point source. SPECT acquisitions for both Lu-177 and Tc-99m point sources were performed using the 10 projections with 60 sec/projection. The total scan duration for each acquisition was 10 min.

3. Uniform phantom acquisition

We made uniform phantoms using 20 ml disposable plastic syringes. The axial length and internal diam-

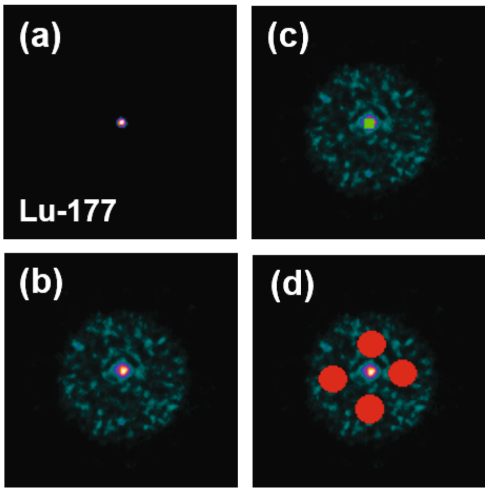

Fig. 2. (Color online) Reconstructed point source image of Lu-177 positioned at center of transaxial FOV (a) without background; (b) with uniform background added; (c) VOIs drawn over background added point image; (d) VOIs drawn over background regions.

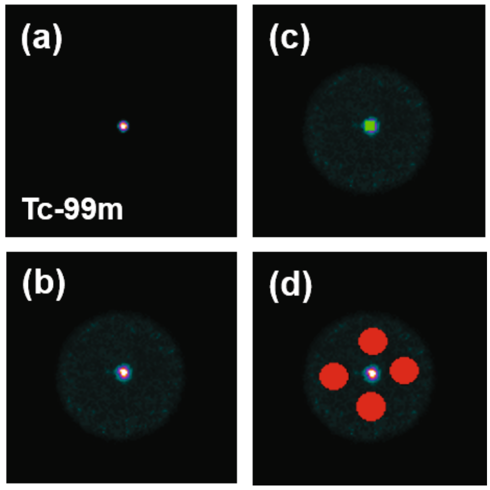

Fig. 3. (Color online) Reconstructed point source image of Tc-99m positioned at center of transaxial FOV (a) without background; (b) with uniform background added; (c) VOIs drawn over background added point image; (d) VOIs drawn over background regions.

eter of uniform phantom were 70 mm and 20 mm respectively. Two uniform phantoms, one containing Lu-177 and another containing Tc-99m were prepared using the activity concentrations of 7.02×10^5 Bq/ml and 7.22×10^5 Bq/ml respectively. The volume of each phantom was 20 ml. The activity was measured in dose calibrator after replacing the needles with syringe cap. All the air was removed while preparing the uniform phantoms. We performed uniform phantom acquisitions using Lu-177 and Tc-99m for: a) uniformity measurement and b) for background adding in the projection data of point sources. For uniformity measurement, large axial FOV (70 mm) was selected and the SPECT data were acquired for 44.92 min (35 projections with 77 sec/projection) for each radionuclide. The energy windows and photopeaks for the both radioisotopes used were same as applied for point source imaging.

4. Adding uniform background to point image

The SPECT projection data of uniform phantoms containing same activity concentrations of Lu-177 and Tc-99m as mentioned in the above section 3 were acquired with limited FOV (14 mm) to match with the point source projection data. But here, the acquisitions were performed for 2 hours for each radionuclide source (10 projections with 12 min/projection) to acquire enough counts. The uniform phantom projection was added to the projection data of point sources to create the uniform background in the reconstructed point source images. The uniform background data was added in such a way that the ratio of reconstructed point peak intensity to the mean background intensity was 10 : 1. The recovery coefficient, reconstructed SPECT uniformity in terms of percentage standard deviation (%SD) were measured from the uniform background added point images.

It has been observed that if a point source image is reconstructed without any background, the reconstruction algorithms can enhance the apparent spatial resolution theoretically and it is not considered as reliable data [27]. Particularly, when using no background, the measured FWHM has the potential to be rendered meaningless as it can approach the voxel size at a very large number of iterations. Hence, we added non-zero background to the point source data before reconstruction to mimic the real in vivo imaging conditions [28].

5. Image reconstruction

All the SPECT point source and uniform phantom images were reconstructed using iterative image reconstruction software, HiSPECT NG (Scivis GmbH, Germany) provided with the NanoSPECT/CT system. Iterative reconstruction for pinhole geometry has ability to correct for image degrading effects and provide better quantitative accuracy than analytical reconstruction methods [29,30]. The point source imaging data were reconstructed in a $120 \times 120 \times 68$ matrix with voxel size of 0.30 mm $\times$ 0.30 mm $\times$ 0.30 mm. This voxel size was recommended for the mouse whole body standard aperture used in this study. The point source images (with and without adding uniform background) were reconstructed with increasing numbers of iterations from three to thirty and the Gaussian filter was kept at its minimum value for spatial resolution measurement. However, we applied 35% Gaussian filter during the reconstruction of point source data for the measurement of recovery coefficient and uniformity.

The SPECT images of uniform phantom were reconstructed using the matrix size of $80 \times 80 \times 204$ and voxel size of 0.45 mm $\times$ 0.45 mm $\times$ 0.45 mm. The image were reconstructed with increasing number of iterations for the uniformity measurement. We applied 35% Gaussian filter during the image reconstruction of uniform phantoms. We use similar reconstruction parameters during the preclinical SPECT imaging of mouse.

6. Performance Evaluation

A. Recovery coefficient and uniformity measurement

The recovery coefficient (RC) and reconstructed SPECT uniformity were measured from the uniform background added point source images (central point in radial direction) of Lu-177 and Tc-99m using Eqs. (1) and (2) respectively. The volume of interests (VOIs) were drawn over each points and background areas using MRIcro tool as shown in Figs. 2 and 3. A cubic VOI (3.38 mm^3) containing 125 voxels was drawn over the point source image. For background area, four cylindrical VOIs were drawn each with the diameter and height of 4.5 mm and 1.5 mm respectively. The total number of voxels in the four cylindrical VOIs was 3240. In Eq. (1), $C_{recon\ point}$ is the average counts in the VOIs of reconstructed point image, $C_{recon\ bkg}$ is the average of the background VOIs and $R_{point/bkg}$ is the ratio of peak intensity of point to the average intensity of the background (10 : 1). The measured RC and %SD with increasing iteration numbers were plotted.

The %SDs were also measured from uniform phantom images of Lu-177 and Tc-99m using different iteration numbers. The VOIs were drawn over the central portion of uniform phantom images for uniformity measurements as shown in Figs. 4(a) and 4(b).

$$\mathrm{RC} = \frac{(C_{recon\ point}/C_{recon\ bkg})}{R_{point/bkg}} \times 100\%, \qquad (1)$$

$$\%\ \mathrm{SD} = \frac{\mathrm{SD}}{\text{mean voxel value}} \times 100\%. \qquad (2)$$

B. Spatial resolution measurement

The spatial resolutions of the NanoSPECT/CT camera for mouse aperture was measured in the term of full width at half of maximum (FWHM). The National Electrical manufacturers Association (NEMA) recommends filtered back-projection (FBP) reconstruction method for spatial resolution measurement, however FBP method was not provided with the reconstruction software available with our system. Therefore, we

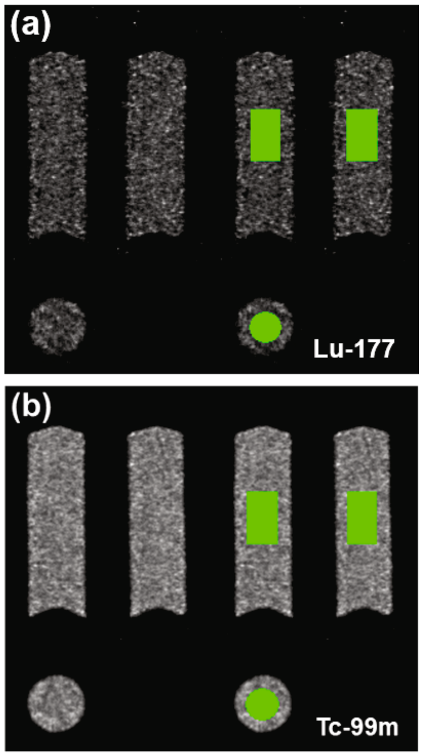

Fig. 4. (Color online) Reconstructed SPECT images of uniform phantoms containing Lu-177 (a) and Tc-99m (b). VOIs were drawn over the central portion of the phantom images.

measured FWHM values using iterative reconstruction methods (HiSPECT NG). The spatial resolutions at each points in axial, radial and tangential direction were measured for Lu-177 and Tc-99m point sources with and without adding uniform background. We first analyzed the relationship between the recovery coefficient and uniformity measured from background added point source image with increasing number of iterations to find the optimum iteration value. Finally, we applied that iteration value for the measurement of the spatial resolutions for both radioisotopes.

C. System sensitivity measurement

The sensitivity (cps/MBq) of the mouse aperture in axial and radial direction was measured using the projection data of Lu-177 and Tc-99m point sources acquired at different positions using Eq. (3). In this equation, N is the total counts measured, T_0 and T_s are the activity measurement time and image acquisition start time respectively, T_{half} is the half-life of radioisotope used, T_d is the scan duration of point source and A_0 is the initial

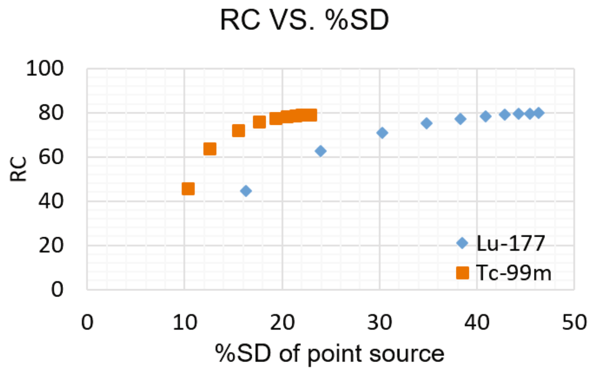

Fig. 5. (Color online) Scattered plot between recovery coefficients (RCs) and %SDs measured from reconstructed point source image with increasing number of iterations (3 to 30) for Lu-177 and Tc-99m. Iteration numbers are denoted by shapes in the figure where first shape indicates 3 iterations, second shape indicates 6 and so on up to 30 iterations.

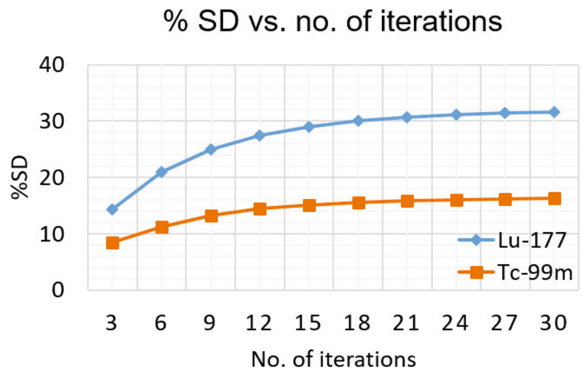

Fig. 6. (Color online) The relationship between %SDs of uniform phantom images and the number of iterations (3 to 30) for Lu-177 and Tc-99m.

activity in the point source.

$$\text{Sensitivity } (S) = \frac{N \times \exp^{\ln(2)\times(T_s - T_0)/T_{half}}}{T_d \times A_0} \quad (3)$$

D. Calibration factor measurement

Calibration factor for Lu-177 was measured using reconstructed uniform phantom image for the conversion of counts to activity (Bq). VOIs were drawn over the uniform phantom image as shown in Fig. 4(a). Mean VOI value (counts/voxel) were noted and the counts per milliliter (counts/ml) was measured which was further corrected for decay. Calibration factor (Bq/counts) was estimated by dividing the initial activity concentration (Bq/ml) in the phantom to the measured counts/ml.

III. RESULTS AND DISCUSSION

1. Recovery coefficient and uniformity

We measured recovery coefficients and percentage standard deviations of Lu-177 and Tc-99m from uniform background added point source images positioned at the center of transaxial FOV. Here, %SD uniformity is acquired from the background of point source imaging. In Fig. 5, we observed that more than 70% Lu-177 activity has been recovered at nine iterations with uniformity of 30% SD. The similar result was observed with Tc-99m source where more than 72% Tc-99m activity was recovered at nine iterations with less than 16% SD as shown in Fig. 5. With increasing iteration numbers, recovery coefficient for both Lu-177 and Tc-99m improved very slightly and reached to the plateau after 15 iterations (Fig. 5). At 30 iterations, recovery coefficients measured for Lu-177 and Tc-99 were 79% and 80% respectively. Compared to Tc-99m, Lu-177 showed poor uniformity however, the recovery coefficient for Lu-177 was comparable to Tc-99m.

We also measured the reconstructed SPECT uniformity of uniform phantoms with increasing iteration numbers. As shown in Fig. 6, we found that the image of uniform phantoms reconstructed with nine iterations resulted with the standard deviations of 25% and 13% for Lu-177 and Tc-99m respectively. We observed poor uniformity for Lu-177 when compared to that of Tc-99m at nine iterations. However, the uniformity was acceptable when using six iterations. Therefore, we can conclude that six iterations might be adequate to be used during the image reconstruction of SPECT imaging of mouse. Although the uniformity improved, the recovery coefficient may decrease with lower iterations if we refer to the point source uniformity analysis (Fig. 5). The uniformity of Lu-177 imaging can be improved by increasing the scan duration to acquire sufficient counts.

Harteveld *et al.* [10] used NEMA NU 4 phantom in a U-SPECT-II small animal SPECT to compare the relationship of activity recovery coefficient and uniformity at different iteration numbers for Tc-99m. They found that when the number of iterations was increased, recovery coefficient increased however, noise in the uniform phantom region was also increased.

2. Spatial Resolution

The Lu-177 and Tc-99m point source imaging data acquired in both axial and transaxial FOVs were reconstructed with and without adding background. After analyzing the relationship between recovery coefficient and uniformity of point source with increasing number of iterations (Fig. 5), we found that the nine iterations would

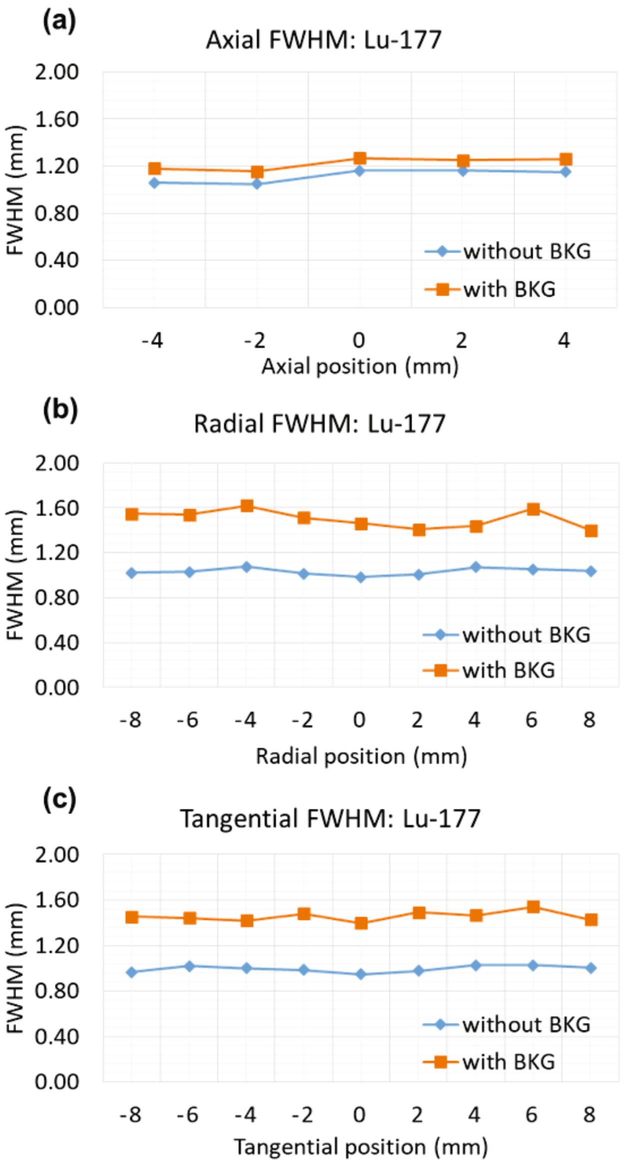

Fig. 7. (Color online) FWHM values measured from Lu-177 point sources positioned at center and other positions with and without adding uniform background in axial (a), radial (b) and tangential (c) directions. BKG, Background.

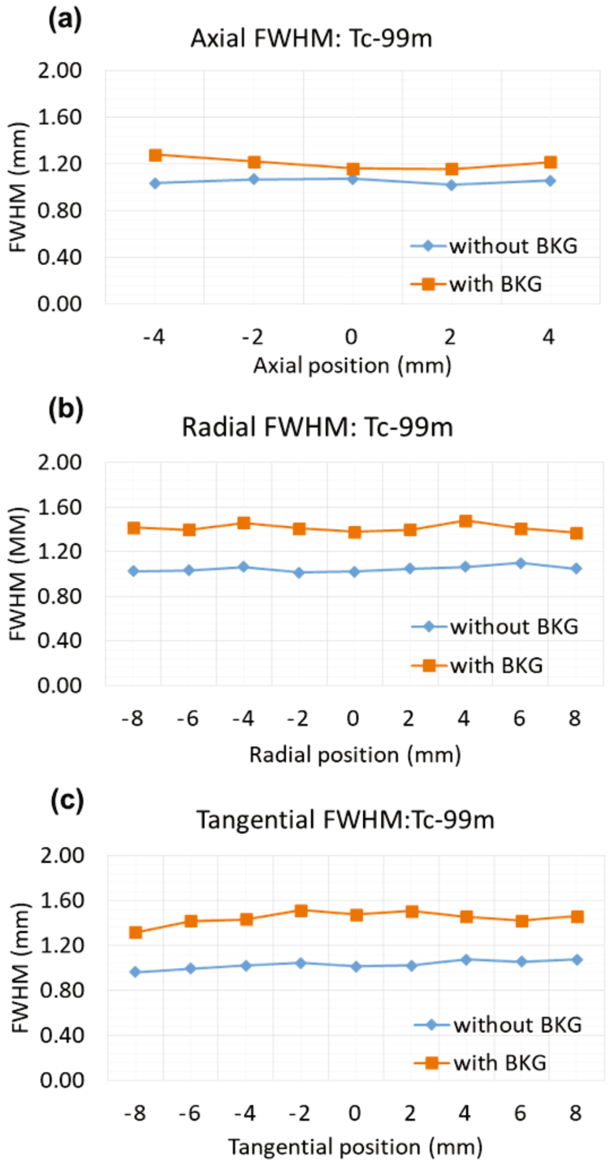

Fig. 8. (Color online) FWHM values measured from Tc-99m point sources positioned at center and other positions with and without adding uniform background in axial (a), radial (b) and tangential (c) directions. BKG, Background.

be more appropriate to measure the reconstructed spatial resolutions from point sources. The FWHM values at center of FOV in axial, radial and tangential direction without adding background were 1.16 mm, 0.98 mm and 0.95 mm respectively for Lu-177 and 1.07 mm, 1.02 mm and 1.02 mm respectively for Tc-99m when using nine iterations. We finally measured the FWHM values for all point source images at different positions (offsets from the center of FOVs) along axial, radial and tangential direction using the same iteration number as shown in Figs. 7 and 8. We did not observe a large difference ($< 10\%$) in position dependency of spatial resolutions measured at other positions in any direction for both radioisotopes (Figs. 7 and 8).

We also measured the FWHM values for both Lu-177 and Tc-99m point sources after adding uniform background and compared the results with those without background. As shown in the Figs. 7 and 8, it can be observed that the spatial resolution deteriorated when the uniform background was added to the point source images. The maximum deteriorations in axial, radial and tangential direction were 10%, 34% and 34% respectively for Lu-177 and 19%, 26% and 32% for Tc-99m.

Schramm *et al.* [12] measured the spatial resolution of series of dedicated multipinhole apertures including the mouse aperture (NSP-108-M14-WB) used in our study.

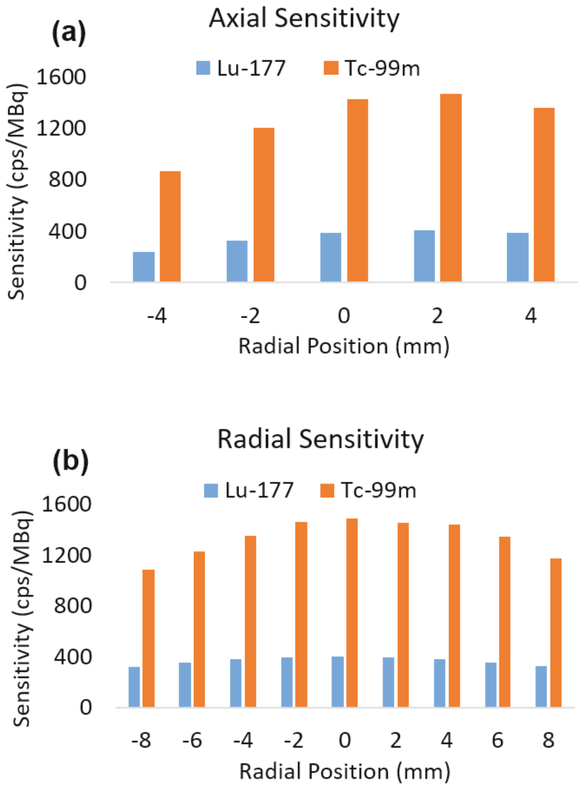

Fig. 9. (Color online) System sensitivities measured from Lu-177 and Tc-99m point source projection data acquired at different positions in axial (a) and transaxial (b) FOVs.

They measured the maximum FWHM value of 1 mm for Tc-99m. In separate study, Cheng *et al.* [13] measured the spatial resolution of NanoSPECT/CT for Tc-99m using smaller version of the Jaszczak mini hot spot phantom, with hot rods of 1.2 to 1.7 mm. They estimated the spatial resolution of 1.2 mm by recognizing the smallest visible size of hot rods in phantoms. Spatial resolution measured in both studies [12, 13] were very similar to FWHM values for Tc-99m obtained in our study.

3. System Sensitivity

We measured the sensitivity for mouse aperture using Lu-177 point source projection data acquired at different positions in axial and transaxial FOVs. We also measured the sensitivity for Tc-99m and compared the results with that of Lu-177 as shown in Fig. 9. We found that the sensitivities of both radioisotopes were the highest at the center of FOVs. The measured sensitivities at the center of axial and tranaxial FOVs were 389 and 401 cps/MBq respectively for Lu-77 and 1426 and 1489 cps/MBq respectively for Tc-99m. We also observed that and the sensitivities of radionuclides gradually decreased as the source moved from the center towards the periphery in both axial and radial directions. The lowest sensitivities for Lu-177 (240 cps/MBq) and Tc-99m (890 cps/MBq) were noted at -4 mm offset from the center in axial FOV. In transaxial FOV, the lowest sensitivities measured for Lu-177 and Tc-99m were 323 and 1082 cps/MBq respectively at -8 mm from the center. The sensitivity of Lu-177 was almost three times less when compared with that of Tc-99m. One of the reasons for low sensitivity of Lu-177 is the low abundance of 208 keV gamma photons, which is only 11% of all disintegrations.

Schramm *et al.* [12] reported the average and peak sensitivities of Tc-99m for standard mouse aperture to be 1200 and 2200 cps/MBq. The average sensitivity measured in their study was very similar to our results obtained at the center of transaxial FOV. In another study, Cheng *et al.* [13] measured the sensitivity of NanoSPECT/CT for Tc-99m using Lucite calibration phantom. They obtained the sensitivity of 622 cps/MBq, which was almost 60% less, compared to the maximum sensitivity measured in our study.

4. Calibration factor

The reconstructed pixel intensity value of Lu-177 phantom image was given in counts. For quantitative analysis and for dosimetry purpose, the counts need to be converted into activity. The measured calibration factor from reconstructed uniform phantom image of Lu-177 was 10.85 Bq/counts. However, this measured calibration factor is not constant and should be measured each time before performing preclinical imaging. Moreover, the calibration factor varies from scanner to scanner. Our NanoSPECT/CT system was already calibrated for Tc-99m source hence, the pixel intensity value for Tc-99m phantom image was given in kBq. Consequently, there was no need to measure the calibration factor for Tc-99m.

We performed the detailed evaluation of performance parameters of multipinhole mouse aperture of NanoSPECT/CT system for Lu-177 and Tc-99m using point source imaging and uniform phantom studies. There are no such study performed earlier for Lu-177 however, very limited number of studies have been published to evaluate the quantitative accuracy of this system using Tc-99m. We found that the results obtained for Tc-99m in our study were very similar to those published by various authors [10, 12, 13]. We used identical point source and uniform phantom, and the imaging conditions were also kept similar for both Lu-177 and Tc-99m studies. Hence, we believed that the results obtained for all the performance parameters (recovery coefficient, reconstructed SPECT uniformity, reconstructed spatial resolution and system sensitivity) evaluated in this study for Lu-177 radionuclide are reliable.

IV. CONCLUSION

Accurate quantitative imaging must be considered as an essential part of the internal dosimetry procedure. Therefore, all these performance parameters evaluated in this study play crucial role in the accuracy of activity quantification while performing pre- and post-therapy SPECT imaging of mouse for personalized dosimetry. Our study investigated the relationship between activity recovery and reconstructed image uniformity at different iteration numbers. The recovery coefficient of more than 70% was achieved for Lu-177 at optimum noise level when nine iterations were used. The spatial resolutions of Lu-177 with and without adding uniform background were comparable to that of Tc-99m in all directions. System sensitivity for Lu-177 was almost three times less than that of Tc-99m however, it is adequate to obtain quantitatively accurate SPECT images for personalized dosimetry.

ACKNOWLEDGMENTS

This work was supported by grants from the National Research Foundation of Korea (NRF) funded by the Korean Ministry of Science and ICT (Grant Nos. NRF-2014M3C7034000 and NRF-2016R1A2B3014645).

REFERENCES

[1] B. L. Franc, P. D. Acton, C. Mari and B. H. Hasegawa, J. Nucl. Med. **49**, 1651 (2008).
[2] S. Park, U. Jung, S. Lee, D. Lee and C. Kim, Biomed. Eng. Lett. **7**, 121 (2017).
[3] J. S. Lee, G. Kovalski, T. Sharir and D. S. Lee, J. Nucl. Cardiol. DOI: https://doi.org/10.1007/s12350-017-0979-8 (2017).
[4] M. G. Pomper and J. S. Lee, Curr. Pharm. Des. **11**, 3247 (2005).
[5] F. J. Beekman and B. Vastenhouw, Phys. Med. Biol. **49**, 4579 (2004).
[6] Y. J. Lee, D. H. Kim, Y. C. Rhee and H. J. Kim, J. Korean Phys. Soc. **64**, 1737 (2014).
[7] N. U. Schramm *et al.*, IEEE Trans. Nucl. Sci. **50**, 315 (2003).
[8] N. Schramm *et al.*, J. Nucl. Med. **47**, 233 (2006).
[9] F. P. Difilippo, Phys. Med. Biol. **53**, 4185 (2008).
[10] A. A. Harteveld *et al.*, J. Nucl. Med. **52**, 1646 (2011).
[11] F. Forrer *et al.*, Eur. J. Nucl. Med. Mol. Imaging. **33**, 1214 (2006).
[12] N. Schramm *et al.*, J. Nucl. Med. **48**, 436 (2007).
[13] D. Cheng *et al.*, Bioconjug. Chem. **21**, 1565 (2010).
[14] C. M. Finucane, I. Murray, J. K. Sosabowski, J. M. Foster and S. J. Mather, Int. J. Mol. Imaging. **2011**, 1 (2011).
[15] S. Deleye *et al.*, Eur. J. Nucl. Med. Mol. Imaging. **40**, 744 (2013).
[16] K. Zukotynski, H. Jadvar, J. Capala and F. Fahey, Biomark. Cancer. **8**, 35 (2016).
[17] D. S. Lee, H. J. Im and Y. S. Lee, Nanomedicine. **11**, 795 (2015).
[18] G. Paganelli *et al.*, Eur. J. Nucl. Med. Mol. Imaging. **41**, 1845 (2014).
[19] A. Romer *et al.*, Eur. J. Nucl. Med. Mol. Imaging. **41**, 214 (2014).
[20] S. Ezziddin *et al.*, Eur. J. Nucl. Med. Mol. Imaging. **41**, 925 (2014).
[21] W. A. van der Zwan *et al.*, Eur. J. Endocrinol. **172**, R1 (2015).
[22] E. Ilan *et al.*, J. Nucl. Med. **56**, 177 (2015).
[23] A. Dash, S. Chakraborty, M. R. Pillai and F. F. Knapp, Cancer Biother. Radiopharm. **30**, 47 (2015).
[24] K. Kim and S. J. Kim, Nucl. Med. Mol. Imaging. DOI: https://doi.org/10.1007/s13139-017-0505-6 (2017).
[25] S. Shcherbinin, H. Piwowarska-Bilska, A. Celler and B. Birkenfeld, Phys, Med. Biol. **57**, 5733 (2012).
[26] E. Mezzenga *et al.*, PLoS One. **12**, 1 (2017).
[27] Y. Yang *et al.*, Phys. Med. Biol. **49**, 2527 (2004).
[28] K. Gong, S. R. Cherry and J. Qi, Phys. Med. Biol. **61**, N193 (2016).
[29] P. P. Bruyant, J. Nucl. Med. **43**, 1343 (2002).
[30] V. Israel-Jost *et al.*, IEEE Trans. Med. Imaging. **25**, 158 (2006).